Demographic inference through approximate-Bayesian-computation skyline plots

Miguel Navascués[1,2]**, Raphaël Leblois**[1,2]**, and Concetta Burgarella**[3]

[1]**INRA, UMR CBGP, F-34988 Montferrier-sur-Lez, France**
[2]**Institut de Biologie Computationnelle, F-34090 Montpellier, France**
[3]**IRD, UMR DIADE, F-34394 Montpellier, France**

Corresponding author:
Miguel Navascués[1]

Email address: miguel.navascues@inra.fr

ABSTRACT

The skyline plot is a graphical representation of estimated past effective population size as a function of time. Its inference is based on models without an a priori assumption on a mathematical function determining the shape of the demographic change, typically a constant piecewise model. Because of this, it is considered to achieve a more realistic description of the complex demographies occurring in natural populations. Currently, there are implementations of the skyline plot based on coalescent samplers and a composite likelihood approach. In the present work we provide an equivalent implementation within the Approximate Bayesian Computation (ABC) framework and provide an assessment of its performance for microsatellite data. The method correctly retrieves the signal of contracting, constant and expanding populations, although the graphical shape of the plot is not always an accurate representation of true demographic trajectory. Because of the flexibility of ABC, similar approaches can be extended to other type of data, to models with multiple populations, or to other parameters that could change through time, such as the migration rate.

Inferring the historical demography of populations by means of genetic data is key to many studies addressing the ecological and evolutionary dynamics of natural populations. Population genetics inference, with appropriate dating, can identify the likely factors (such as climatic events) determining the demography of a species. With enough research resources, this can be done with an outstanding detail (e.g. in humans, reviewed in Nielsen et al., 2017). Demographic inference can also be used to generate null models for the detection of loci under selection (as discussed in Hoban et al., 2016).

At present, most of the methods to estimate demography from genetic data are based on the coalescent. The coalescent (see Wakeley, 2008, for a review) is a mathematical model that describe the rate at which genetic lineages coalesce (i.e. join in a common ancestor) towards the past forming the genealogy of the sample. The coalescence probability depends on the effective population size at each time in the past, that is, the demographic history of the population. Given a genealogy, the coalescent allows calculating the likelihood of the demographic model. Inference is obtained by calculating the likelihood of the model given the data, which requires to integrate over all possible genealogies for the data. This is approximated by means of Monte Carlo algorithms known as coalescent samplers (see review by Kuhner, 2009).

Alternatively, the coalescent can be used to calculate the likelihood of the number of genetic differences for a pair of gene copies under a given demographic model. This can be done for all pairs in a sample to obtain a composite-likelihood (because pairs are not independent and they are related by their genealogy). By ignoring this dependency, the composite-likelihood score can be used as a criterion to estimate the parameters of the model with faster algorithms than the coalescent samplers although with lower performance, particularly regarding confidence intervals (e.g. Navascués et al., 2009; Nikolic and Chevalet, 2014).

Coalescent models can also be used in the likelihood-free framework known as Approximate Bayesian Computation (ABC, Tavaré et al., 1997; Beaumont et al., 2002). In this approach, the likelihood is

substituted by the similarity between the observed data and simulated data generated from a given model. Similarity is usually evaluated by means of a distance between observed and simulated summary statistics. This distance allows select the simulations close to the observed data and reject those too far away. Posterior probability distributions are estimated from the collection of parameter values used in the accepted simulations (see Beaumont, 2010, for a review on ABC).

A classical way to address the estimation of past population size changes by these methods is to assume simple parametric models, such as exponential, logistic or instantaneous demographic change. However, these are sometimes considered too simple to describe the dynamics of real populations. In the skyline plot methods (see Ho and Shapiro, 2011, for a review) the underling demographic model consists in a piecewise constant population size model, i.e. the demographic history consists of several periods of constant size, with instantaneous changes of sizes between each two consecutive periods. The aim is to provide a more flexible framework that could capture the complex demography expected in natural populations. Such models have been implemented in Markov chain Monte Carlo coalescent samplers (software BEAST; Drummond et al., 2005; Minin et al., 2008; Heled and Drummond, 2008), an importance sampling coalescent sampler (Ait Kaci Azzou et al., 2015) for the analysis of sequence data. The incorporation of microsatellites to the software BEAST (Wu and Drummond, 2011) allowed to make skyline plot inference for this type of data (e.g. Allen et al., 2012; Molfetti et al., 2013; Minhós et al., 2016). Also for microsatellite data, a composite-likelihood approach has been developed (R package VarEff; Nikolic and Chevalet, 2014).

It is worth noting that similar piecewise models of inference have been proposed in the context of population genomics (e.g. Li and Durbin, 2011; Terhorst et al., 2016). The methods discussed above assume a set of independent (unlinked) genetic markers. However, if a large proportion of the genome has been sequenced, the studied polymorphism are no independent. Methods such as the Pairwise Sequentially Markovian Coalescent (PSMC, Li and Durbin, 2011) and its successors profit from the additional information from linkage disequilibrium for the inference. We will not further discuss this family of methods because the focus of this work will be on datasets of independent molecular markers, such as microsatellites, which remain reliable markers for low-budget projects. Note, however, the PSMC-like implementation on ABC by Boitard et al. (2016).

The use of the skyline plot in the ABC framework was first proposed in Burgarella et al. (2012). Here, we provide a suite of R scripts (DIYABCskylineplot) to produce approximate-Bayesian-computation skyline plots from microsatellite data and evaluate its performance on simulated pseudo-data. We show the method to be useful to detect population decline and expansion and discuss its limits. ABC skyline plots are then build for four study cases (whale shark, leatherback turtle, Western black-and-white colobus and Temminck's red colobus) and compared with the demographic inference obtained by an alternative full likelihood method.

METHODS

ABC skyline plot

For a demographic skyline plot analysis within the ABC framework, our model consisted of a single population with constant size that instantaneously changes to a new size n times through time. The parameters (from present to past, as in the coalescent model) the present scaled population size $\theta_0 = 4N_0\mu$ (where N_0 is the effective population size in number of diploid individuals and μ is the mutation rate per generation) which changes to θ_1 at time $\tau_1 = T_1\mu$ (where T is the time measured in generations), remains at θ_1 and then it changes to θ_2 at τ_2, and so on, until the last change to θ_n at τ_n. Note that other models and parametrization could have been used for our purpose, as in the alternative model that we present in the supplementary material section S1.2.

The objective of a standard ABC analysis would be to estimate the posterior distribution for each parameter of the model. In our case, the parameters $\{(\theta_i, \tau_i); i \in [0,n]\}$ have been treated as nuisance parameters and we focused on inferring from them the trajectory of the scaled effective population size along time, $\theta(t)$, as in Drummond et al. (2005). In order to approximate $\theta(t)$ we select m times of interest, $\{t_j; j \in [1,m]\}$. Given a simulation k with parameters $\{(\theta_{k,i}, \tau_{k,i}); i \in [0,n_k]\}$, derived parameters $\{\theta_k(t_j); j \in [1,m]\}$ are obtained as follows: $\theta_k(t_j) = \theta_{k,i}$ for i satisfying the condition $\tau_{k,i} \leq t_j < \tau_{k,i+1}$ (see Supplementary Figure S1 for some examples). For each t_j, inference of the derived parameters $\theta(t_j)$ were obtained following standard ABC procedures as described elsewhere (e.g. Beaumont et al., 2002).

Median and 95% highest posterior density (HPD) intervals of derived parameters $\theta(t_j)$ were be used to draw ABC skyline plots.

Simulations with different number of population size changes can be used for inference because of the use of derived parameters $\theta(t_j)$, which are common to all models. We set the prior probability on the number of constant size periods to be Poisson distributed with $\lambda = \ln(2)$ as in Heled and Drummond (2008). This gives equal prior probability to stable populations (a single period of constant size) and changing populations (two or more periods). Thus, posterior probability on the number of periods may be used to discriminate between stable and changing demographies by estimating the Bayes factor of one period (constant population size) *versus* several demographic periods (variable population size). Posterior probabilities of contrasting models can be obtained by logistic regression as described elsewhere (Beaumont, 2008).

We implemented this approach in a suite of R scripts (R Core Team, 2017) that we named DIYABCskylineplot (Navascués, 2017). For each simulation the number of population size changes is sampled using the prior probabilities. Via command line version of DIYABC (v2.0, Cornuet et al., 2014), parameter values, $\{(\theta_{k,i}, \tau_{k,i}); i \in [0, n_k]\}$, are sampled from the prior distribution, coalescent simulations are performed and summary statistics are calculated [mean across loci of the number of alleles, N_a; heterozygosity, H_e; variance of allele size, V_a, and Garza and Williamson (2001) statistic, M]. In addition, the *Bottleneck* statistic (ΔH; Cornuet and Luikart, 1996), which compares the expected heterozygosity given the allele frequencies with the expected heterozygosity given the observed number of alleles, is calculated in R from the summary statistics provided by DIYABC. Derived parameter values, $\{\theta_k(t_j); j \in [1, m]\}$, are calculated from the reference table (i.e. table of original parameters and summary statistics values for all simulations) produced by DIYABC and their posterior probability distributions are estimated in R using the *abc* package (Csilléry et al., 2012).

Simulations

The method described above was evaluated on simulated data (pseudo observed data-set, POD) of contracting and expanding populations. Declining populations had a present effective size of $N_0 = 100$ diploid individuals that changed exponentially until time T, which had a value of 10, 50, 100 or 500 generations in the past, reaching an ancestral population sizes of N_A, which had a value of 1000, 10 000 or 100 000 individuals. Expanding populations had a present population size of N_0 with a value of 1000, 10 000 or 100 000 diploid individuals, which changed exponentially until reaching the size of the ancestral population $N_A = 100$ at time T, which had a value of 10, 50, 100 or 500 generations in the past. For times older than T, the population size is constant at N_A for all scenarios. In addition, we simulated three constant population size scenarios with N taking a value of 1000, 10 000 or 100 000. Equivalent scenarios were also evaluated in Girod et al. (2011) and Leblois et al. (2014). PODs were generated for 50 individuals genotyped at 30 microsatellite loci evolving under a generalised stepwise mutation model (GSM, Slatkin, 1995). Mutation rate was set to $\mu = 10^{-3}$ and P_{GSM} to 0.00, 0.22 or 0.74 (P_{GSM} is the parameter of a geometric distribution determining the mutation size in number of repeats). One hundred replicates (i.e. PODs) were run for each scenario. Therefore, the mutation scaled parameter values are for $\theta = 4N\mu$: 0.4, 4, 40 or 400 and for $\tau = T\mu$: 0.01, 0.05, 0.1 or 0.5. PODs were obtained using the coalescent simulator fastsimcoal (Excoffier and Foll, 2011).

Every POD was analysed with the same set of prior probability distributions that largely includes all parameter values of simulations. Scaled effective size parameters, θ_i, were taken from a log-uniform distribution in the range $(10^{-3}, 10^4)$ and scaled times, τ_i, from a log-uniform distribution in the range $(2.5 \times 10^{-4}, 4)$. A uniform prior in the range $(0,1)$ was used for mutational parameter P_{GSM}. For each replicate of each scenario, we obtained the skyline plot (median and 95%HPD intervals of the $\theta(t_j)$ posterior distributions) and estimated the Bayes factor between constant size and variable demography by using logistic regression. Estimates of the mutational parameter P_{GSM} were also obtained for each POD. For each scenario, mean absolute error, bias and proportion of times the true value falls outside the credibility interval were estimated.

Data sets

In addition to PODs, four real data-sets from the literature were re-analysed with the ABC skyline plot described above: data from the whale shark (*Rhincodon typus*; Vignaud et al., 2014b), the leatherback turtle (*Dermochelys coriacea*; Molfetti et al., 2013) and two species of colobus monkeys (the Western black-and-white colobus, *Colobus polykomos*, and the Temminck's red colobus, *Procolobus badius*

temminckii; Minhós et al., 2016). Data were analysed with the same prior distributions as PODs except for the colobus monkeys datasets, which consist of tetranucleotide markers. Previous evidence suggests that tetranucleotide microsatellite mutations are mainly of only one repeat unit (e.g. Leopoldino and Pena, 2003; Sun et al., 2012). In order to incorporate this prior knowledge, half of the simulations had $P_{GSM} = 0$ (i.e. a strict stepwise mutation model, SMM) and the other half had the parameter sampled from a uniform distribution in the range (0,1).

For comparison, demographic history of the four real data sets was also explored using the MIGRAINE software (http://kimura.univ-montp2.fr/~rousset/ Migraine.htm) under the model of a single panmictic population with an exponential change in population size. To infer model parameters, MIGRAINE uses coalescence-based importance sampling algorithms under a maximum likelihood framework Leblois et al. (2014) using OnePopVarSize model. In this model, MIGRAINE estimates present and ancestral scaled population sizes ($\theta_0 = 4N_0\mu$ and $\theta_A = 4N_A\mu$) and the scaled time of occurrence of the past change in population size ($D = T/4N$, going backward from sampling time, when the population size change began). The past change in population size is deterministic and modelled using an exponential growth or decline that starts at time D. Before time D, scaled population size is stable and equal to θ_A. MIGRAINE allows departure from the strict SMM by using a GSM with parameter P_{GSM} for the geometric distribution of mutation sizes. Finally, detection of significant past change in population size is based on the ratio of population size ($\theta_{ratio} = \theta_0/\theta_A$). $\theta_{ratio} > 1$ corresponds to a population expansion and $\theta_{ratio} < 1$ to a bottleneck. If no significant demographic change is obtained, MIGRAINE is run again under a model of stable demography (a single value of θ) for parameter estimation. For the whale shark data set, MIGRAINE analysis was already done in Vignaud et al. (2014b). For the leatherback turtle, MIGRAINE was run using 20 000 trees, 200 points at each iteration and a total of 16 iterations. For the colobus monkeys, we considered 2 000 trees, 400 points at each iteration and a total of 8 iterations.

RESULTS

Simulations

The general behavior of the method can be described from three example scenarios (contraction with $\theta_0 = 0.4$, $\theta_1 = 40$, $\tau = 0.1$, expansion with $\theta_0 = 40$, $\theta_1 = 0.4$, $\tau = 0.1$ and constant size with $\theta = 40$; mutational model with $P_{GSM} = 0.22$) and their results will be presented in the main text. These examples correspond to intermediate parameter values; results for all simulations are available in the supplementary material.

The main output of the analysis is the graphical representation (i.e. the skyline plot) of the inferred demographic trajectory. It consists in a plot with three curves, representing the point estimate (median) and 95%HPD interval of θ through time. Skyline plots obtained from PODs are congruent with the true underlying demography simulated (Figure 1), except in the less favorable scenarios with very recent or very small changes in population size (Supplementary Figures S2–S8). Although the trajectory of the posterior median of θ and the true trajectory share the same trend (declining, increasing or constant), they sometimes differ in magnitude or time-scale. This disparity is more prominent for bottleneck scenarios.

For a quantitative criterion to assert demographic change we have explored the value of posterior probabilities for constant and variable population size models, similar to the scheme proposed by Heled and Drummond (2008). These probabilities (summarised as Bayes factors in Figure 2) proved to be useful for distinguishing bottleneck and expansion scenarios from demographic stability, although with lower performance for less favorable scenarios (Supplementary Figures S9–S15). Constant size scenarios show no evidence for size change.

Changes in population size were co-estimated with the mutational model parameter P_{GSM}. Mean absolute error, bias and proportion of replicates for which the true value was outside the 95%HPD interval are reported in Table 1 for the three example scenarios and in Table S1 for all simulations. Estimates from expanding and stable populations show a relatively low error and bias and a good coverage of the credibility interval (except in the strict SMM case). However, estimates from declining populations show higher error and bias.

Real Data

The ABC analyses show evidence of population expansion for the whale shark (BF=59.62) and the leatherback turtle (BF=16.65); no evidence for population size changes in the black-and-white colobus (BF=0.58) and some evidence for a bottleneck in the red colobus (BF=2.63), with their respective skyline

plots reflecting such trends (Figure 3). Results from MIGRAINE support the same trends, with θ_{ratio} significantly higher than one for the whale shark and the leatherback turtle, significantly lower than one for the red colobus and no significantly different than one for the black-and-white colobus (Supplementary Table S3). Scaled population size estimates through time are also in accord, except for the leatherback turtle, where MIGRAINE result suggest a more ancestral expansion of much greater magnitude.

Regarding the mutational model, a large proportion of multi-step mutations seems to be present in all datasets, with P_{GSM} estimates: $\hat{P}_{GSM} = 0.55$ (95%HPD=0.46–0.62) for the whale shark; $\hat{P}_{GSM} = 0.50$ (95%HPD=0.38–0.60) for the leatherback turtle; $\hat{P}_{GSM} = 0.43$ (95%HPD=4.05×10^{-3}–0.53) for the black-and-white colobus; and $\hat{P}_{GSM} = 0.18$ (95%HPD=0.02–0.75) for the red colobus (see also Supplementary Figure S16). Although very low values of P_{GSM} are included in the credibility interval from the colobus analyses, the GSM is favoured over the SMM when an ABC model choice analysis is performed (BF=57.50 for the black-and-white colobus and BF=10.01 for the red colobus). These results are congruent with estimates of P_{GSM} by MIGRAINE (Supplementary Table S3).

DISCUSSION

The ability of the ABC skyline plot to detect changes in population size varies largely across the different scenarios evaluated. The evidence for demographic change was often strong (even very strong) in declining and expanding populations. However, demographic changes of small magnitude and close to the present were the hardest to detect. Recent or small magnitude events leave a weak signal in the genetic data and are also hard to identify for alternative methods (see Girod et al., 2011; Leblois et al., 2014; Nikolic and Chevalet, 2014). In any case, the method shows to be conservative, since most analysis of stable populations yielded negative or little evidence for demographic change.

Skyline-plot main appeal is to depict demographic trajectories not bounded to a mathematical function; thus, potentially reflecting more realistically the demography of natural populations. However, our results show that plotted trajectories loosely reflect of the true demography, particularly those of contracting populations. The match between the true and inferred demographic trajectory was good for constant size populations and for some expanding populations. Ancestral and current population sizes (the extremes of the skyline plot) were also retrieved accurately for favourable scenarios. Nevertheless, the shape of the curve representing the transition between them was a poor representation of the true demographic trajectory in many cases. While this conclusion is specific for the implementation presented in this work, it calls to caution for the interpretation of results from other methods yielding smooth skyline plots (e.g. Heled and Drummond, 2008; Nikolic and Chevalet, 2014). A superficial comparison with the methods implemented in R package VarEff (Nikolic and Chevalet, 2014) and BEAST (v 1.8 Heled and Drummond, 2008) seems to indicate that their output can suffer from a similar problem on accuracy (see Supplemantary Figure S19).

It is worth to mention that bottlenecked populations, which show the greatest discrepancy between the skyline plot and the true demographic curve, are also the scenarios for which the mutational parameter P_{GSM} was inferred with larger bias. Similar patterns of summary statistics are produced with large P_{GSM} values and with a bottleneck (e.g. large allele size variance, see Supplementary Table S2), which may difficult an accurate joint inference of demography and mutational model. This difficulty to distinguish between scenarios with frequent multi-step mutations and contracting populations also explains the reduction in power to detect some bottleneck cases such as those with large P_{GSM} value and strong population size decline (see Supplementary Figures S11). A negative effect on demographic inference due to mutational model misspecification has been reported also for alternative methods (see Girod et al., 2011; Leblois et al., 2014; Nikolic and Chevalet, 2014).

These results highlight the interest of using complimentary inference methods and data. In the four real-data populations, their demographies have been previously studied in the original publications. In addition to the MIGRAINE analysis on microsatellite data, Vignaud et al. (2014b) inferred a population expansion for the whale shark by using Bayesian skyline plot analysis on mitochondrial DNA sequence data, corroborating the signal of expansion for this species. In the case of the leatherback turtle, the previous analyses were less conclusive (Molfetti et al., 2013). An extended Bayesian skyline plot on microsatellite data suggested a recent expansion, but it was found not significant, and the skyline plot on mitochondrial DNA data did not show any demographic change. On contrast, analysis of microsatellite data with MSVAR (a coalescent sampler approach, Beaumont, 1999; Storz and Beaumont, 2002) suggested a strong population decline. However, it must be noted that MSVAR assumes a strict SMM, which can

lead to biases in the demographic estimates when microsatellite mutations include a substantial proportion of multi-step changes (Girod et al., 2011; Faurby and Pertoldi, 2012). Our estimates of the P_{GSM} parameter and the two-phase model used in BEAST suggest a strong departure from the SMM and lead us to favour the hypothesis of population expansion. Finally, the original analysis of the two colobus species found significant evidence of population decline for both of them (Minhós et al., 2016). Again, this evidence was obtained from MSVAR and the extended Bayesian skyline plot implemented in BEAST assuming a SMM. Despite the prior results suggesting that tertranucleotide microsatellite mutations add or remove a single repeat, our analyses (ABC skyline plot and MIGRAINE) rejected the SMM for the black-and-white colobus. This explains the difference between their results and our demographic inference, which supports a constant population size for this population.

A common problem for the inference of population size changes is the presence of population structure or gene flow. Most methods aiming the detection of population size change often assume the analysis of a single, independent population, but violating of these assumptions usually conduce to false detection of bottlenecks (e.g. Heller et al., 2013; Nikolic and Chevalet, 2014, for skyline plot approaches). We expect the same effect on the skyline plot analysis in the implementation we present here. However, distinguishing between population structure and population decline in the ABC framework is possible with the appropriate summary statistics (Peter et al., 2010) that can be included in future implementations of the ABC skyline plot.

Indeed, the ease to incorporate new summary statistics and models is the prime interest for implementing the skyline plot in the ABC framework. Models with multiple populations can be simulated and skyline plots for each of the populations estimated. Extensions to other molecular markers can also be developed and already exist for genomic data (e.g. Boitard et al., 2016). Finally, other demographic parameters could be subject to variations with time, such as the migration rate (Pool and Nielsen, 2009), and could be inferred with a similar scheme. To sum up, there is potential to develop such approach in different directions, to address new questions in future research.

In this work we presented a detailed description on how to compute an approximate-Bayesian-computation skyline plot and assessed its performance on stable and changing simulated populations characterized with microsatellite markers. Its power to detect the signal of demographic change is similar to alternative methods. However, its potential ability to depict more realistically the demography of natural populations must not be overrated. Still it offers a complementary analysis to other methods and there is great potential to develop it to cover other models and genetic data.

ACKNOWLEDGMENTS

REFERENCES

Ait Kaci Azzou, S., Larribe, F., and Froda, S. (2015). A new method for estimating the demographic history from DNA sequences: an importance sampling approach. *Frontiers in Genetics*, 6:259.

Allen, J. M., Miyamoto, M. M., Wu, C.-H., E. Carter, T., Ungvari-Martin, J., Magrini, K., and Chapman, C. A. (2012). Primate DNA suggests long-term stability of an African rainforest. *Ecology and Evolution*, 2(11):2829–2842.

Beaumont, M. A. (1999). Detecting population expansion and decline using microsatellites. *Genetics*, 153(4):2013–2029.

Beaumont, M. A. (2008). Joint determination of topology, divergence time, and immigration in population trees. In Matsumura, S., Forster, P., and Renfrew, C., editors, *Simulation, Genetics, and Human Prehistory*, McDonald Institute Monographs, pages 135–154. McDonald Institute for Archaeological Research, Cambridge.

Beaumont, M. A. (2010). Approximate Bayesian computation in evolution and ecology. *Annual Review of Ecology, Evolution, and Systematics*, 41(1):379–406.

Beaumont, M. A., Zhang, W., and Balding, D. J. (2002). Approximate Bayesian computation in population genetics. *Genetics*, 162(4):2025–2035.

Boitard, S., Rodríguez, W., Jay, F., Mona, S., and Austerlitz, F. (2016). Inferring population size history from large samples of genome-wide molecular data - an approximate Bayesian computation approach. *PLOS Genetics*, 12(3):e1005877.

Burgarella, C., Navascués, M., Zabal-Aguirre, M., Berganzo, E., Riba, M., Mayol, M., Vendramin, G. G., and González-Martínez, S. C. (2012). Recent population decline and selection shape diversity of taxol-related genes. *Molecular Ecology*, 21(12):3006–3021.

Cornuet, J. M. and Luikart, G. (1996). Description and power analysis of two tests for detecting recent population bottlenecks from allele frequency data. *Genetics*, 144(4):2001–2014.

Cornuet, J.-M., Pudlo, P., Veyssier, J., Dehne-Garcia, A., Gautier, M., Leblois, R., Marin, J.-M., and Estoup, A. (2014). DIYABC v2.0: a software to make approximate Bayesian computation inferences about population history using single nucleotide polymorphism, DNA sequence and microsatellite data. *Bioinformatics*, 30(8):1187–1189.

Csilléry, K., François, O., and Blum, M. G. B. (2012). abc: an R package for approximate Bayesian computation (ABC). *Methods in Ecology and Evolution*, 3(3):475–479.

Drummond, A. J., Rambaut, A., Shapiro, B., and Pybus, O. G. (2005). Bayesian coalescent inference of past population dynamics from molecular sequences. *Molecular Biology and Evolution*, 22(5):1185–1192.

Excoffier, L. and Foll, M. (2011). fastsimcoal: a continuous-time coalescent simulator of genomic diversity under arbitrarily complex evolutionary scenarios. *Bioinformatics*, 27(9):1332–1334.

Faurby, S. and Pertoldi, C. (2012). The consequences of the unlikely but critical assumption of stepwise mutation in the population genetic software, MSVAR. *Evolutionary Ecology Research*, 14(7):859–879.

Garza, J. C. and Williamson, E. G. (2001). Detection of reduction in population size using data from microsatellite loci. *Molecular Ecology*, 10(2):305–318.

Girod, C., Vitalis, R., Leblois, R., and Fréville, H. (2011). Inferring population decline and expansion from microsatellite data: A simulation-based evaluation of the msvar method. *Genetics*, 188(1):165–179.

Heled, J. and Drummond, A. J. (2008). Bayesian inference of population size history from multiple loci. *BMC Evolutionary Biology*, 8(1):289.

Heller, R., Chikhi, L., and Siegismund, H. R. (2013). The confounding effect of population structure on Bayesian skyline plot inferences of demographic history. *PLoS ONE*, 8(5):e62992.

Ho, S. Y. W. and Shapiro, B. (2011). Skyline-plot methods for estimating demographic history from nucleotide sequences. *Molecular Ecology Resources*, 11(3):423–434.

Hoban, S., Kelley, J. L., Lotterhos, K. E., Antolin, M. F., Bradburd, G., Lowry, D. B., Poss, M. L., Reed, L. K., Storfer, A., and Whitlock, M. C. (2016). Finding the genomic basis of local adaptation: Pitfalls, practical solutions, and future directions. *The American Naturalist*, 188(4):379–397.

Jeffreys, H. (1961). *Theory of Probability*. Oxford University Press, Oxford, 3rd edition.

Kuhner, M. K. (2009). Coalescent genealogy samplers: windows into population history. *Trends in Ecology & Evolution*, 24(2):86–93.

Leblois, R., Pudlo, P., Néron, J., Bertaux, F., Beeravolu, C. R., Vitalis, R., and Rousset, F. (2014). Maximum-likelihood inference of population size contractions from microsatellite data. *Molecular Biology and Evolution*, 31(10):2805–2823.

Leopoldino, A. M. and Pena, S. D. J. (2003). The mutational spectrum of human autosomal tetranucleotide microsatellites. *Human Mutation*, 21(1):71–79.

Li, H. and Durbin, R. (2011). Inference of human population history from individual whole-genome sequences. *Nature*, 475(7357):493–496.

Minhós, T., Chikhi, L., Sousa, C., Vicente, L. M., Ferreira da Silva, M., Heller, R., Casanova, C., and Bruford, M. W. (2016). Genetic consequences of human forest exploitation in two colobus monkeys in Guinea Bissau. *Biological Conservation*, 194:194–208.

Minin, V. N., Bloomquist, E. W., and Suchard, M. A. (2008). Smooth skyride through a rough skyline: Bayesian coalescent-based inference of population dynamics. *Molecular Biology and Evolution*, 25(7):1459–1471.

Molfetti, E., Torres Vilaça, S., Georges, J.-Y., Plot, V., Delcroix, E., Le Scao, R., Lavergne, A., Barrioz, S., dos Santos, F. R., and de Thoisy, B. (2013). Recent demographic history and present fine-scale structure in the Northwest Atlantic leatherback (*Dermochelys coriacea*) turtle population. *PLoS ONE*,

8(3):e58061.

Navascués, M. (2017). DIYABCskylineplot v1.0.1: A suite of R scripts to perform a Approximate Bayesian Computation Skyline Plot. doi:10.5281/zenodo.267182.

Navascués, M., Hardy, O., and Burgarella, C. (2009). Characterization of historical demographic expansions from pairwise comparisons of haplotypes using linked mirosatellites. *Genetics*, 181(3):1013–1019.

Nielsen, R., Akey, J. M., Jakobsson, M., Pritchard, J. K., Tishkoff, S., and Willerslev, E. (2017). Tracing the peopling of the world through genomics. *Nature*, 541(7637):302–310.

Nikolic, N. and Chevalet, C. (2014). Detecting past changes of effective population size. *Evolutionary Applications*, 7(6):663–681.

Peter, B. M., Wegmann, D., and Excoffier, L. (2010). Distinguishing between population bottleneck and population subdivision by a Bayesian model choice procedure. *Molecular Ecology*, 19(21):4648–4660.

Pool, J. E. and Nielsen, R. (2009). Inference of historical changes in migration rate from the lengths of migrant tracts. *Genetics*, 181(2):711–719.

R Core Team (2017). *R: A Language and Environment for Statistical Computing*. R Foundation for Statistical Computing, Vienna, Austria.

Slatkin, M. (1995). A measure of population subdivision based on microsatellite allele frequencies. *Genetics*, 139(1):457–462.

Storz, J. F. and Beaumont, M. A. (2002). Testing for genetic evidence of population expansion and contraction: an empirical analysis of microsatellite DNA variation using a hierarchical bayesian model. *Evolution*, 56(1):154.

Sun, J. X., Helgason, A., Masson, G., Ebenesersdóttir, S. S., Li, H., Mallick, S., Gnerre, S., Patterson, N., Kong, A., Reich, D., and Stefansson, K. (2012). A direct characterization of human mutation based on microsatellites. *Nature Genetics*, 44(10):1161–1165.

Tavaré, S., Balding, D. J., Griffiths, R. C., and Donnelly, P. (1997). Inferring coalescence times from DNA sequence data. *Genetics*, 145(2):505–518.

Terhorst, J., Kamm, J. A., and Song, Y. S. (2016). Robust and scalable inference of population history from hundreds of unphased whole genomes. *Nature Genetics*, advanced online.

Vignaud, T. M., Maynard, J. A., Leblois, R., Meekan, M. G., Vázquez-Juárez, R., Ramírez-Macías, D., Pierce, S. J., Rowat, D., Berumen, M. L., Beeravolu, C., Baksay, S., and Planes, S. (2014a). Data from: Genetic structure of populations of whale sharks among ocean basins and evidence for their historic rise and recent decline. Dryad Digital Repository. doi:10.5061/dryad.489s0.

Vignaud, T. M., Maynard, J. A., Leblois, R., Meekan, M. G., Vázquez-Juárez, R., Ramírez-Macías, D., Pierce, S. J., Rowat, D., Berumen, M. L., Beeravolu, C., Baksay, S., and Planes, S. (2014b). Genetic structure of populations of whale sharks among ocean basins and evidence for their historic rise and recent decline. *Molecular Ecology*, 23(10):2590–2601.

Wakeley, J. (2008). *Coalescent Theory: An Introduction*. Roberts & Company Publishers.

Wu, C.-H. and Drummond, A. J. (2011). Joint inference of microsatellite mutation models, population history and genealogies using transdimensional Markov chain Monte Carlo. *Genetics*, 188(1):151–164.

DATA ACCESSIBILITY

Code for DIYABCskylineplot is available on ZENODO (doi:10.5281/zenodo.267182) and on GitHub (http://github.com/mnavascues/DIYABCskylineplot) including code to automatically simulate pseudo-data. Data from whale sharks is available at DRYAD database (Vignaud et al., 2014a).

AUTHOR CONTRIBUTIONS

MN and CB conceived and designed the work. MN developed the code. MN, RL and CB analysed the data and discussed the results. MN and RL wrote the article. All authors read and approved the final manuscript.

TABLES AND FIGURES

Table 1. Estimation of mutational parameter P_{GSM}

model	θ_0	θ_1	τ	P_{GSM}	MAE	bias	out of CI
contraction	0.4	40	0.1	0.22	0.14	0.13	0.01
expansion	40	0.4	0.1	0.22	0.05	-0.04	0.05
constant size	40			0.22	0.06	-0.03	0.00

MAE: mean absolute error; out of CI: proportion outside credibility interval (95%HPD). Estimates from 100 replicates.

Figure 1. ABC Skyline plots: simulations. Superimposed skyline plots (median in black, and 95%HPD interval in dark (upper limit) and pale (lower limit) grey of the posterior probability distribution for $\theta(t)$) from 100 replicates for example contraction ($\theta_0 = 0.4$, $\theta_1 = 40$, $\tau = 0.1$), expansion ($\theta_0 = 40$, $\theta_1 = 0.4$, $\tau = 0.1$) and constant size ($\theta = 40$) scenarios with mutational model $P_{GSM} = 0.22$. True demography is shown in orange. Note that present is at $\tau = 0$ (left).
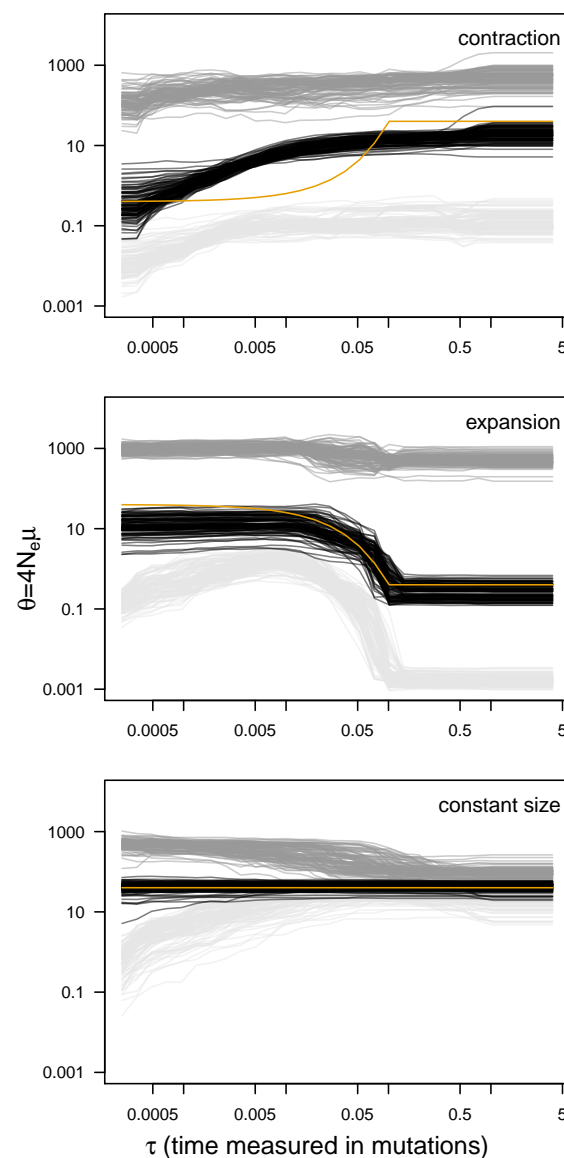
Figure 2. Evidence for variable population size. Bayes factor distribution (boxplot) from 100 replicates for example contraction ($\theta_0 = 0.4$, $\theta_1 = 40$, $\tau = 0.1$), expansion ($\theta_0 = 40$, $\theta_1 = 0.4$, $\tau = 0.1$) and constant size ($\theta = 40$) scenarios with mutational model $P_{GSM} = 0.22$. For reference, Jeffreys (1961) scale is given for the evidence against constant size.
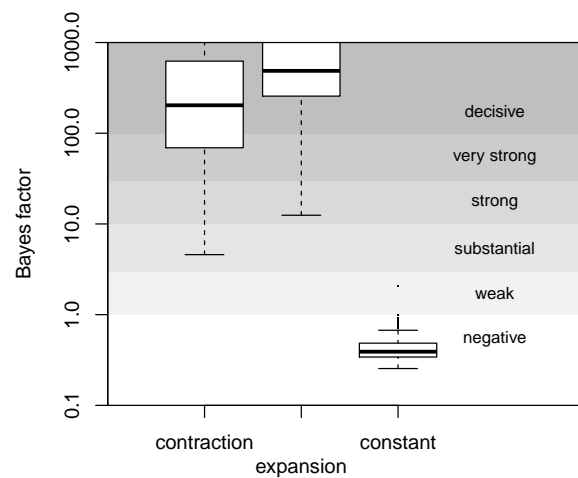
Figure 3. ABC Skyline plots: real data. Skyline plots (median in black, and 95%HPD interval in grey of the posterior probability distribution for $\theta(t)$) for whale shark, leatherback turtle, Western black-and-white colobus and Temminck's red colobus. Bayes Factors (BF) are reported for the variable *versus* constant size model. Demographic trajectories based on parameters point estimates from MIGRAINE analysis are shown with a dashed green line for reference. Note that present is $\tau = 0$ (left).